In situ determination of the remotely sensed reflectance and the absorption coefficient: closure and inversion

Andrew H. Barnard, J. Ronald V. Zaneveld, and W. Scott Pegau

We tested closure between *in situ* radiometric and absorption coefficient measurements by using a nearly backscattering-independent remote-sensing reflectance model that employs the remote-sensing reflectance at three wavelengths. We show that only a small error is introduced into the closure model when the proper functional relationships of f/Q and the backscattering is taken to be a constant when using the sea-viewing wide field-of-view sensor wavelengths 443, 490, and 555 nm. A method of inverting the model to obtain the absorption coefficient by use of simple linear spectral relationships of the absorption coefficient is provided. The results of the model show that the independent measurements of reflectance and absorption obtain closure with a high degree of accuracy. © 1999 Optical Society of America

OCIS codes: 280.0280, 300.1030, 290.0290, 290.1350.

1. Introduction

The proliferation of advanced noninvasive instruments for the measurement of the in-water apparent and inherent optical properties of the oceans has increased over the past ten years. The intercomparison of these *in situ* measurements is important in the determination of optical closure and the scale problem.[1,2] Resolution of these issues provides assurance that the small-scale inherent optical properties (IOP's) determined with flow-through devices can be used in radiative transfer schemes to determine the apparent optical properties (AOP's) which are determined from daylight observations. In this paper we describe a method to test in-water measurements of remote-sensing reflectance and absorption for closure based on radiative transfer.

In recent years there has been a focused effort to derive new methods for the determination of the IOP's of the oceans from ocean color satellite measurements.[3–5] This effort has been driven in part by an increased ability to measure the in-water optical properties more accurately and effectively, allowing for more-detailed studies of the optical property relationships. Correspondingly, there has been an increase in the development of ocean color satellites, with new ocean color sensors planned in the future in addition to the sea-viewing wide field-of-view sensor (SeaWiFS), which is currently operational. Thus we are now in a position where we are able to validate inversion using *in situ* data and satellite estimates. A key component to this validation is the issue of closure between the in-water measurements of reflectance and the IOP's.

However, most remote-sensing reflectance algorithms must make assumptions about the angular dependency of the underwater light field and the backscattering component, as these parameters are not easily measured or currently well understood. It is the purpose of this research to derive a model that greatly minimizes the influence of these parameters. We show that, by using two ratios with three different wavelengths of the remote-sensing reflectance, the influence of the spectral dependency of the backscattering coefficient and the angular dependence of the underwater light field is greatly reduced. The ability of three-band reflectance ratios to remove the angular dependency of the water-leaving radiance was originally noted by Campbell and Esaias.[6] In this study we extend the results of their study to show that utilizing reflectance ratios at three wavelengths also minimizes the spectral dependence of the backscattering coefficient.

The authors are with the College of Oceanic and Atmospheric Sciences, Oregon State University, 104 Oceanographic Administration Building, Corvallis, Oregon 97331. The e-mail address for A. H. Barnard is abarnard@oce.orst.edu.

2. Theory and Approach

A. Remote-Sensing Reflectance R_{rs}

The connection between the IOP's and the AOP's is through the equation of radiative transfer, which solves for the radiance distribution as a function of depth when the absorption and scattering properties of the seawater as well as the incident radiance distribution are known. The irradiance reflectance $R(\lambda)$, defined as the upwelling irradiance (E_u) normalized by the downwelling irradiance (E_d) just below the surface, is related to the absorption and backscattering coefficients as defined by Preisendorfer[7]:

$$R(\lambda) = \frac{E_u(\lambda)}{E_d(\lambda)} = f(\lambda)\,\frac{b_b(\lambda)}{a(\lambda)}, \qquad (1)$$

where f is the parameter relating irradiance reflectance to the ratio of the backscattering b_b and absorption a coefficients radiance (see Appendix A for a complete list of symbols). However, as ocean color satellites remotely sense the upwelled radiance, Eq. (1) subsequently has been modified to look at the ratio of the upwelling radiance to the downwelling irradiance. This is most commonly known as the remote-sensing reflectance[8,9] and is defined as

$$R_{rs}(\lambda) \equiv \frac{R(\lambda)}{Q(\lambda)} = \frac{L_u(\lambda)}{E_d(\lambda)} \cong \frac{f(\lambda)}{Q(\lambda)}\,\frac{b_b(\lambda)}{a(\lambda)}, \qquad (2)$$

where Q is the ratio of the upwelling irradiance and the nadir radiance.

Much discussion has been involved in determining the f/Q ratio, which depends on the shape of the upwelling light field and the volume-scattering function.[10–12] Rather than having to approximate the value of this ratio, we want to formulate an expression for the remote-sensing reflectance, which depends solely on the IOP's of the water column.

B. f/Q Considerations

The f parameter, which depends on the shape of the light field and the volume-scattering function, is typically assumed to be equal to 0.33, although it has been shown to exhibit a total range of 0.25–0.55 for most oceanic environments.[9] The Q factor, which is an indicator of the shape of the upwelling light field, can vary over an order of magnitude, with Q equal to π for a totally diffuse radiance distribution.[9] However, Morel and Gentili[9] found that f/Q is well behaved spectrally, with much of the variation in f canceled by the fluctuation in Q. Zaneveld[13] has also shown that the f parameter is directly proportional to Q, and that unless there is significant multiple scattering, the dependence of L_u/E_d on Q is weak over most remote-sensing angles. These observations can be used to derive a function that significantly reduces the contribution of the f/Q ratio.

By utilizing two ratios of R_{rs} at three wavelengths, we can derive the following equation:

$$R_{rs3}(\lambda_1, \lambda_2, \lambda_3) = \frac{R_{rs}(\lambda_1)}{R_{rs}(\lambda_2)}\bigg/\frac{R_{rs}(\lambda_2)}{R_{rs}(\lambda_3)}$$

$$\cong \frac{\dfrac{f}{Q}(\lambda_1)\dfrac{f}{Q}(\lambda_3)\dfrac{b_b}{a}(\lambda_1)\dfrac{b_b}{a}(\lambda_3)}{\left[\dfrac{f}{Q}(\lambda_2)\right]^2\left[\dfrac{b_b}{a}(\lambda_2)\right]^2}. \qquad (3)$$

Based on Monte Carlo simulations for nadir radiance, solar zenith angle of 30.0°, and a chlorophyll concentration of 0.1 mg m^{-3}, Morel and Gentili[9] computed the f/Q values to be approximately 0.089, 0.088, and 0.0875 for the wavelengths 443, 490, and 555 nm (see their Fig. 5). The triple ratio of the f/Q parameter by use of these wavelengths is approximately 1.006. Thus, if the spectral behavior of f/Q is linear or nearly so, and the center wavelength (λ_2) is nearly equally spaced between the other two, one can show that only a small error is induced by assuming that the triple ratio of f/Q is equal to one. Given the Q-like behavior of f, and the weak wavelength dependence of f/Q, we assume the f/Q triple ratio in Eq. (3) to be a constant equal to one, reducing Eq. (3) to

$$R_{rs3}(\lambda_1, \lambda_2, \lambda_3) = \frac{R_{rs}(\lambda_1)}{R_{rs}(\lambda_2)}\bigg/\frac{R_{rs}(\lambda_2)}{R_{rs}(\lambda_3)} \cong \frac{\dfrac{b_b}{a}(\lambda_1)\dfrac{b_b}{a}(\lambda_3)}{\left[\dfrac{b_b}{a}(\lambda_2)\right]^2}. \qquad (4)$$

If we assume that the remotely sensed portion of the water column is homogeneous, i.e., that the IOP's are homogeneously distributed over the remote-sensing depth, we can separate the backscattering and absorption components such that

$$R_{rs3}(\lambda_1, \lambda_2, \lambda_3) = \frac{R_{rs}(\lambda_1)}{R_{rs}(\lambda_2)}\bigg/\frac{R_{rs}(\lambda_2)}{R_{rs}(\lambda_3)}$$

$$\cong \frac{b_b(\lambda_1)b_b(\lambda_3)}{b_b{}^2(\lambda_2)}\frac{a^2(\lambda_2)}{a(\lambda_1)a(\lambda_3)}. \qquad (5)$$

We now have derived an equation for a remotely sensed reflectance parameter R_{rs3} purely in terms of the backscattering and the absorption coefficients by assuming a weak spectral dependence of f/Q and a homogeneous vertical distribution of the IOP's over the remote-sensing depth.

C. Backscattering Component

The scattering parameter that is relevant to the remotely sensed radiance is not simply the backscattering coefficient, but rather a weighted integral of the volume-scattering function in the backward direction.[8,12,13] This function cannot be measured easily at present. Furthermore the angular distribution of the backscattering coefficient is

not well known at this time. Thus it is of interest to derive an equation for the remote-sensing reflectance that is nearly independent of the backscattering coefficient. In the text below we examine the spectral dependence of the backscattering triple ratio. For simplification in what follows we set

$$b_{br3} = b_{br3}(\lambda_1, \lambda_2, \lambda_3) = \frac{b_b(\lambda_1)b_b(\lambda_3)}{b_b{}^2(\lambda_2)}. \qquad (6)$$

The backscattering coefficient depends on the water and its particulate components, such that

$$b_b(\lambda) = b_{bw}(\lambda) + b_{bp}(\lambda), \qquad (7)$$

where b_{bw} is the backscattering coefficient of water and b_{bp} is the backscattering coefficient of particles. The backscattering coefficient of water has a $\lambda^{-4.32}$ spectral dependence,[14] whereas a $\lambda^{-\eta}$ spectral dependence is typically assumed for the backscattering by particles.[15-19] Thus

$$b_{bw}(\lambda) = b_{bw}(\lambda_r)\left(\frac{\lambda}{\lambda_r}\right)^{-4.32}, \quad b_{bp}(\lambda) = b_{bp}(\lambda_r)\left(\frac{\lambda}{\lambda_r}\right)^{-\eta}, \quad (8)$$

where λ_r is a reference wavelength. Substituting Eqs. (8) into Eq. (6) and taking λ_2 as the reference wavelength, we can rewrite the triple backscattering ratio in the following manner:

$$b_{br3} = \frac{\left[b_{bw}(\lambda_2)\left(\frac{\lambda_1}{\lambda_2}\right)^{-4.32} + b_{bp}(\lambda_2)\left(\frac{\lambda_1}{\lambda_2}\right)^{-4.32}\right]\left[b_{bw}(\lambda_2)\left(\frac{\lambda_3}{\lambda_2}\right)^{-\eta} + b_{bp}(\lambda_2)\left(\frac{\lambda_3}{\lambda_2}\right)^{-\eta}\right]}{\left[b_{bw}(\lambda_2) + b_{bp}(\lambda_2)\right]^2}. \qquad (9)$$

For simplification in what follows we set $b_{bw} = b_{bw}(\lambda_2)$, and $b_{bp} = b_{bp}(\lambda_2)$ as the wavelength dependence has been eliminated. Equation (9) can then be reduced to

$$b_{br3} = \frac{\left(\frac{b_{bw}}{b_{bp}}\right)^2\left(\frac{\lambda_1\lambda_3}{\lambda_2{}^2}\right)^{-4.32} + \frac{b_{bw}}{b_{bp}}\left[\left(\frac{\lambda_1}{\lambda_2}\right)^{-\eta}\left(\frac{\lambda_3}{\lambda_2}\right)^{-4.32} + \left(\frac{\lambda_1}{\lambda_2}\right)^{-\eta}\left(\frac{\lambda_3}{\lambda_2}\right)^{-4.32}\right] + \left(\frac{\lambda_1\lambda_3}{\lambda_2{}^2}\right)^{-\eta}}{\left(\frac{b_{bw}}{b_{bp}} + 1\right)^2}. \qquad (10)$$

Equation (10) can be evaluated for typical oceanic situations, where b_b ranges from particle-dominated backscattering to water dominated, $0 \leq b_{bw}/b_{bp} \leq 2.5$, and where the spectral scattering dependency varies from $0 \leq \eta \leq 2$.

In practice, the choice of λ_1, λ_2, and λ_3 depends on the wavelengths that are available on *in situ* and satellite sensors. For the purposes of this paper we examine the 443-, 490-, and 555-nm wavelengths, as *in situ* reflectance and IOP's are commonly measured
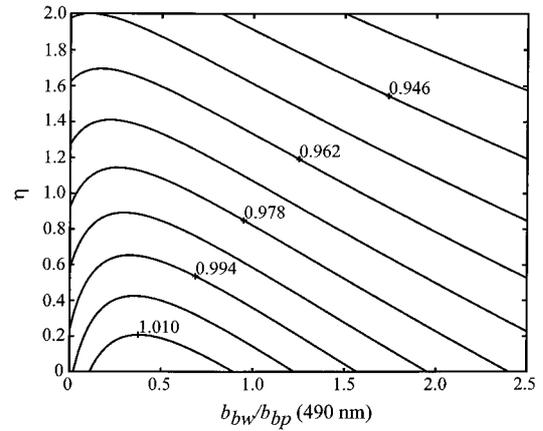
Fig. 1. Contour of the backscattering triple ratio b_{br3} as a function of the shape of the particle backscattering η and the water-to-particle backscattering ratio at 490 nm (b_{bw}/b_{bp}), computed with Eq. (9) and the wavelengths 443, 490, and 555 nm.

at these wavelengths and are also available on the SeaWiFS ocean color satellite. Figure 1 shows the dependence of b_{br3} on η and b_{bw}/b_{bp} calculated with $\lambda_1 = 443$, $\lambda_2 = 490$, and $\lambda_3 = 555$ nm in Eq. (10). The value of b_{br3} ranges from 0.93 to 1.02, with the greatest variation in b_{br3} with η occurring when the back-scattering by particles is greater than the water backscattering (i.e., $b_{bw}/b_{bp} < 1.0$). When one chooses a constant value for b_{br3} nominally equal to 0.975, an error of maximally 4.5% is made for most realistic ocean water types. This error is well within the typical error bars for the *in situ* determination of remote-sensing reflectance and the absorption coefficient. It can thus be seen that for all practical purposes, b_{br3} can be considered to be a constant when the 443-, 490-, and 555-nm wavelengths are considered. Note that in the formulation of the backscattering triple ratio, no additional assumptions were made as to the type or size distribution of the particles. As one can readily see from Fig. 1, fluctuations

in the backscattering coefficient that are due to variations in the spectral shape and magnitude are greatly reduced in the triple ratio expression.

The value of b_{br3} in Eq. (10) could be computed with *in situ* measurements of the backscattering coefficient. However, such devices are only recently being developed.[20] To evaluate the accuracy of the above simplifications, we computed the value of b_{br3} by modeling the backscattering coefficient based on the in-water profiles of the particulate scattering coefficient b_p. We modeled the profiles of total backscattering at each wavelength as

$$b_b(\lambda, z) = b_{bp}(\lambda, z) + b_{bw}(\lambda) \cong \tilde{b}_b b_p(\lambda, z) + 0.5 b_w(\lambda),$$

(11)

where $\tilde{b}_b$ is the probability of the particle backscattering and b_w is the scattering coefficient for pure water. The value of the $\tilde{b}_b$ parameter has been modeled by others based on various assumptions. In a model by Morel *et al.*[21] for case I waters, $\tilde{b}_b$ decreased logarithmically from 2.2% in low-chlorophyll, oligotrophic waters to 0.2% in high-chlorophyll, eutrophic waters. In a similar model by Gordon *et al.*,[8] the particle backscattering probability varied from 2% in low-chlorophyll waters to 0.5% in high-chlorophyll waters. Ahn *et al.*,[18] using monocultures of algae, indicated that the spectral dependence of the backscattering probability is a function of cell size and pigmentation of the individual species and, for the species they studied, was always less than 0.5%. As the data set used in this study is typically somewhere between oligotrophic to eutrophic oceanic environments (see Section 3), we chose a value of $\tilde{b}_b = 1\%$. Although we expect that the spectral dependence of $\tilde{b}_b$ will depend on algal concentration and size distribution, to a first approximation we assume that there is no spectral dependence over the wavelength range used in this study. Thus in this method we assume a spectral dependence and, to some extent, a particle type and size distribution by choosing a constant $\tilde{b}_b$ value.

D. Closure

Substituting the above formulations of the backscattering component b_{br3} we can now replace Eq. (5) by

$$R_{rs3}(\lambda_1, \lambda_2, \lambda_3) \cong b_{br3} \frac{a^2(\lambda_2)}{a(\lambda_1) a(\lambda_3)}.$$

(12)

Given nearly simultaneous profiles of the upwelling radiance, downwelling irradiance, and the total absorption, relation (12) can be tested for closure with the above assumptions. This model thus allows for the direct comparison (and prediction) of a radiometric quantity R_{rs3} with an IOP, the absorption triple ratio. Testing the equivalency of these expressions in the major purpose of this paper.

E. Inversion

Clearly if relation (12) is correct to within acceptable limits, and b_{br3} is set to a constant, the remote-sensing reflectance spectrum can be used to determine the triple ratio of the absorption coefficient. If for a given region or time period there exist functional relationships between the absorption at these three wavelengths, so that $a(\lambda_1) = f_1[a(\lambda_2)]$ and $a(\lambda_3) = f_3[a(\lambda_2)]$, we can then set

$$R_{rs3}(\lambda_1, \lambda_2, \lambda_3) \cong b_{br3} \frac{a^2(\lambda_2)}{f_1[a(\lambda_2)] f_3[a(\lambda_2)]}.$$

(13)

In this formulation, the triple reflectance ratio is expressed as function of $a(\lambda_2)$ only. Provided that regional or global relationships between $a(\lambda_1)$, $a(\lambda_2)$, and $a(\lambda_3)$ can be found, we can use relation (13) to invert R_{rs3} to determine the absorption coefficient at λ_2.

Any functional form for the spectral absorption coefficient can be utilized in relation (13), including separating the absorption coefficient into its respective components (i.e., water, particles, yellow matter). Most semianalytical remote-sensing algorithms provide for these functional relationships in terms of the individual components of the absorption coefficient.[3–5] However, our interest is not in determining the most accurate method of inversion, but rather to demonstrate how this algorithm minimizes the uncertainty involved in estimating the parameters that are most difficult to measure, namely the f/Q and the b_b component. Therefore in this paper we present simplistic absorption coefficient functionalities to provide an example of how the model can be used for inversion to obtain the spectral absorption coefficient.

In a recent paper by Barnard *et al.*[22] it was shown that over a wide range of oceanic environments, simple linear relationships exist between the 443- and 555-nm and the 490-nm absorption coefficients. However, in their paper the linear relationships of the absorption coefficient did not include the contribution by pure water. If consistent linear relationships of the total absorption coefficient (including pure water) exist between these wavelengths from the 70 profiles used in this study, such that

$$f_1[a(490)] = [a(443)] = A[a(490)] + B,$$

$$f_3[a(490)] = [a(555)] = C[a(490)] + D,$$

then we can substitute these functional forms into relation (13) and solve for the absorption coefficient at 490 nm. In this method, as opposed to the presentation given in Barnard *et al.*, we include the offsets B and D in our models to account for the spectral dependence of the absorption coefficient by pure water. Again, we emphasize that simplistic linear functionalities are not likely to be the most accurate way of modeling the spectral absorption coefficient, especially when considering regionalized data sets. However, for our purposes, we utilize them to demonstrate how relation (13) can be used to invert the remotely sensed radiance. Also, substitution of these simple linear models into relation (13) produces the following quadratic equation for the absorption

coefficient at 490 nm, which can be solved easily for given *in situ* measurements of the remotely sensed reflectance:

$$a(490) = \frac{-(AD + BC) \pm \left[\left(AD + BC\right)^2 - 4\left(AC - \frac{b_{br3}}{R_{rs3}}\right)(BD)\right]^{1/2}}{2\left(AC - \frac{b_{br3}}{R_{rs3}}\right)}.$$ (14)

terest are 443, 490, and 555 nm. The remotely sensed reflectance was computed from the profiles of E_d and L_u as in Eq. (2).

3. Data and Measurements

A. Data Sets

Data from six separate research cruises were used to test relation (12) for closure. Four research cruises were carried out in the Gulf of California during the fall of 1995, 1996, and 1997 and the spring of 1998. Optical property data were also collected during the coastal mixing and optics experiment off the Northeast Atlantic Shelf during the fall of 1996 and the spring of 1997. IOP profiles on all cruises were collected by use of the slow descent rate optics platform. This platform typically carries two spectral absorption and attenuation meters, a CTD, and a WETLabs, Inc. modular ocean data and power system to integrate the data streams. Profiles of E_d and L_u and the IOP made within 120 min of each other were selected to minimize temporal and horizontal translation. From these six cruises, 70 temporally and spatially varying profiles of E_d, L_u, and the IOP were used to test relation (12) for closure. The locations and dates for each data set are shown in Table 1.

B. Remote-Sensing Reflectance

We measured profiles of spectral E_d and L_u during both the coastal mixing and the optics experiment cruises and during the 1996 Gulf of California cruise by using a Satlantic SeaWiFS profiling multichannel radiometer (SPMR). A Biospherical profiling reflectance radiometer (PRR-600) was used to collect the irradiance and radiance data during the 1995, 1997, and 1998 Gulf of California cruises. The SPMR and the profiling reflectance radiometer measure downwelling irradiance and upwelling radiance at seven wavelengths. For this study the wavelengths of in-

B. Inherent Optical Properties

We made profiles of the IOP by using a WETLabs, Inc. ac-9 meter, which measures the absorption and beam attenuation coefficients at nine wavelengths. Details on the calibration, deployment, and processing procedures of the absorption data are provided in Barnard *et al.*,[22] Twardowski *et al.*,[23] and WETLabs, Inc. (www.wetlabs.com). The absorption coefficients for pure water[24] were added to the ac-9 measurements to derive the total absorption coefficient. The particulate scattering coefficient was drived from the difference of the beam attenuation and absorption coefficient measurements. The scattering coefficients for pure water utilized in Eq. (11) were obtained from Morel.[14] The wavelengths of interest in this study are the 440-, 488-, and 555-nm bands. Because the ac-9 absorption measurements are determined by use of filters with a 10-nm bandwidth, we assume that these wavelengths are sufficiently similar to the irradiance and radiance wavelengths for comparison.

C. Optical Weighting of Profiles

Both the IOP and the E_d and L_u data were binned to 1-m resolution. Because we are interested in determining if the model achieves closure, we made no effort to extrapolate the radiance and irradiance measurements to just above the sea surface (i.e., 0+). Instead, we computed R_{rs} at the shallowest radiance or irradiance measurement, and then correspondingly adjusted the IOP profiles such that the E_d, L_u, and IOP profiles are measured over the same depth range. One good reason for doing this is to avoid the

Table 1. Data Set Locations and Dates Consisting of 70 IOP and AOP Profiles[a]

Location Description	Date Range	Latitude (°N) Range	Longitude (°W) Range	Number of Profiles
Gulf of California	1–3 December 1995	27.69–27.95	110.96–111.40	6
	31 October–7 November 1996	26.81–28.11	110.13–112.11	18
	16–29 October 1997	24.82–30.22	109.50–114.28	11
	6–16 March 1998	25.57–31.13	110.57–114.52	8
Northeast Atlantic Shelf	18 August–6 September 1996	40.33–40.52	70.47–70.52	23
	26–30 April 1997	40.5	70.49	4

[a]Profiles are separated by less than 20 min.
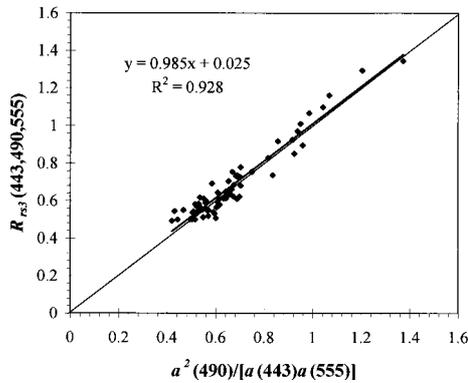
Fig. 2. Triple ratio of the remote-sensing reflectance at 443, 490, and 555 nm determined from *in situ* radiometer measurements versus the triple ratio of the absorption coefficient at 443, 490, and 555 nm determined from *in situ* ac-9 measurements.

Fig. 3. Optically weighted absorption coefficient at 490 nm versus the optically weighted absorption coefficient at 443 nm (filled diamonds) and 555 nm (asterisks) determined from ac-9 measurements. The linear regressions for each wavelength are also shown.

possible uncertainty involved in extrapolating the irradiance and radiance measurements to the surface.

To test the model for closure, we must first address the issue of scales. In Eq. (2) the remote-sensing reflectance was defined to be the ratio of the upwelling radiance to the downwelling irradiance as a function of depth. Therefore the right-hand side of Eq. (2) must be integrated such that it represents an optically weighted absorption measurement for the same water column. We follow the method presented by Zaneveld and Pegau[25] in which the water column is divided into N layers, the optical properties in each layer are homogeneous, and each layer has a light attenuation coefficient H_n that describes the round-trip attenuation of the upwelling and downwelling irradiance through the layer. For each of the corresponding profiles, we computed the optically weighted total absorption coefficient at each of the three wavelengths using

$$\langle a \rangle = \frac{\sum_{n=1}^{N} H_n a_n}{\sum_{n=1}^{N} H_n}, \text{ with } H_n = \frac{L_{u_{n-1}} E_{d_{n-1}} - L_{u_n} E_{d_n}}{L_{u_{n0}} E_{d_{n0}}}.$$
(15)

In our convention, each n layer is 1 m thick, a_n is the average absorption coefficient within each 1-m-thick layer, and L_{u_n} and E_{d_n} are the upwelling radiance and downwelling irradiance at the bottom of each 1-m layer. The subscript 0 is the shallowest AOP sample depth for a given profile. The depth of the 90% light attenuation level at a given wavelength was used as the bottom of the last layer ($n = N$) for each profile. The modeled profiles of the backscattering coefficient were optically weighted in the same manner as the absorption coefficient.

4. Results

A. *In situ* Measurement Closure: Constant b_{br3} Case

Figure 2 shows R_{rs3} versus the triple ratio of the absorption coefficient for the 70 profiles used in this
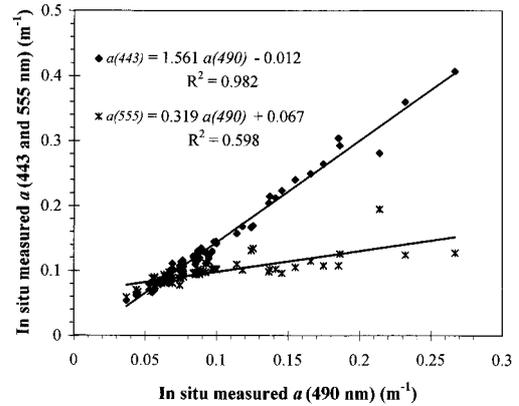
study. Assuming that there are no biases in the model, then the slope of the linear regression of this data would indicate the mean value of b_{br3} for these 70 profiles. The results indicate that the model does achieve closure with an $R^2 = 0.928$ and a standard error of 0.051. The 95% confidence interval on the y intercept of the regression (0.025 ± 0.046) indicates that it is not significantly different from zero. The slope of the linear regression is 0.985 with the 95% confidence interval of ±0.067. Based on the results given in Fig. 1, this value for b_{br3} is well within the expected range. Given that the profiles of the absorption coefficient and R_{rs} were not made concurrently, we expect that the regression would not be perfect because of the temporal and spatial differences between the profiles. Also note that in testing the algorithm for closure, nine *in situ* measurements are used (three wavelengths each of upwelling radiance, downwelling irradiance, and absorption). Inaccuracies in the calibration of each of these measurements may significantly increase the error of the model, especially if the spectral shape of one or more of these parameters is incorrect. Given the good relationship between R_{rs3} and the triple ratio of the absorption coefficient and that the slope of this relationship is well within the expected range of b_{br3}, we conclude that closure between the *in situ* determinations of R_{rs} and the absorption coefficient has been demonstrated.

B. Variable b_{br3} Comparison

Because we demonstrated closure between the *in situ* measurements of remotely sensed reflectance and the absorption coefficient using relation (12), it is of interest to examine the error associated with estimating the value of b_{br3} using *in situ* b_p measurements. In Fig. 1 it was shown that the value of b_{br3} is between 0.93 and 1.02 for most oceanic environments. Recall that the spectral dependence of the backscattering coefficient by particles is known to range from λ^0 for most phytoplankton cells[17,18] to λ^{-2} for the very
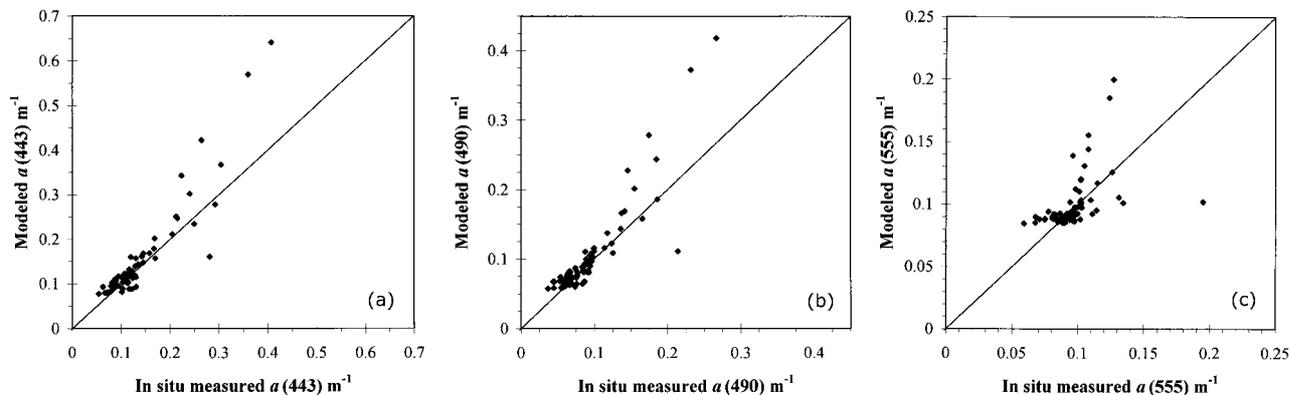
Fig. 4. Predicted absorption coefficient at (a) 443, (b) 490, and (c) 555 nm based on the remote-sensing reflectance triple ratio and the absorption relationships at 443 and 555 nm [see Fig. 3 and Eq. (14)] versus the *in situ* measured absorption coefficient at each of the respective wavelengths.

small particles (0.2–0.5 μm).[19]   Because our data set contains a mixture of both oceanic and near-coastal stations, a λ^{-1} dependence for the backscattering coefficient by particles was assumed.

In the 70 profiles used in this study, the scattering coefficient by particles at 490 nm ranges from 0.103 to 1.344 m^{-1}.   Assuming that b_{bp} is 1% of b_p, then the observed range of b_{bw}/b_{bp} would be expected to range between 0.1 and 1.25.   Thus from Fig. 1 the value of b_{br3} for our data should range from approximately 0.95 to 1.02, with a center value near 0.985.   The mean value for all 70 profiles of the b_{br3} ratio computed with the backscattering coefficient model in Eq. (11) is 1.015 with a standard deviation of 0.027. The modeled backscattering b_{br3} values range from 0.96 to 1.08, with 41% of the values being greater than the highest expected value of b_{br3} (1.02).   The possible causes for these high values of b_{br3} include an inaccurate choice for $\tilde{b}_b$(1%) and instrumental measurement errors of the b_p.   This emphasizes the difficulty in modeling the backscattering component. However, it interesting to note that even with these possible errors, the difference between the value of b_{br3} returned from the regression shown in Fig. 2 and in the modeled b_{br3} is only 0.03.

C.   Inversion to Obtain the Absorption Coefficient

To invert relation (12) to obtain the absorption coefficient at 490 nm, we must provide for the spectral dependence of the absorption coefficient.   Figure 3 shows the absorption coefficient at 490 nm for the 70 profiles used in this study versus the absorption coefficient at 443 and 555 nm.   It is evident that simple linear relationships exist between the total absorption coefficient at 490 nm and at 443 and 555 nm, with the coefficient of variation equal to 0.98 and 0.60, respectively.   The lower coefficient of variation at 555 nm is most likely due to a narrow range of variability in the absorption at 555 nm as compared with the range observed at 490 nm.   These functional relationships of the absorption coefficient were used to invert relation (13) to predict the absorption coefficient at 490 nm based on the measured remote-

sensing reflectance, assuming a constant b_{br3} value of 0.985.   Again, we emphasize that the functional form of these relationships does not necessarily require that they be linear, nor do we expect these relationships to be the most accurate models for the spectral absorption coefficient.   However, use of linear relationships greatly simplifies the inversion to obtain the total absorption coefficient and provides an example of how relation (13) can be used for inversions.   Although this is not an independent test of the model because the functional relationships of the absorption coefficient were derived from the same data set used to test the model for closure, it can provide insight on the influence of b_{br3} on predicting the absorption coefficient.

The results of the inversion model in predicting the spectral absorption coefficient are plotted in Fig. 4, with the associated statistics given in Table 2, and can be summarized as follows.   The absorption coefficient at 443 and 490 nm can be predicted reasonably well with a general tendency to overpredict the absorption values.   However, the predictability of the 555-nm absorption coefficient is poor, which is most likely due to the uncertainty in the 555–490-nm absorption relationship (see Fig. 2).   The predictability of the absorption coefficient at all three wavelengths is lowest at the higher absorption coefficient values, where the predicted value can be as great as a factor of 2 different from the measured value.

In the paper by Barnard *et al.*[22] it was noted that the linear relationships between 443 and 555 nm and the absorption coefficient at 490 nm change when the absorption coefficient at 490 nm is greater than 0.225 m^{-1}.   The change in the relationships was found to occur when the absorption by particles dominated the absorption by dissolved materials.   Indeed, in examining Fig. 3 more closely, it can be seen that for absorption coefficients at 490 nm greater than 0.15 m^{-1}, the predicted values can be different from the measured ones by a factor of 2.   Because our linear models of the spectral absorption coefficient do not provide for the change in the relationships with the increase in the absorption values, the error in the

Table 2. Regression Results of the *in situ* Measured and Modeled Absorption Coefficients[a]

Predicted versus Measured Parameter	Slope	Offset	R^2	Standard Error	95% Confidence Limits	
					Slope	Offset
$a(490)$	1.336	−0.021	0.809	0.030	0.157	0.016
$a(443)$	1.359	−0.031	0.852	0.041	0.137	0.021
$a(555)$	0.538	0.048	0.220	0.019	0.246	0.024
Lee et al.[26]						
$a(440)$ three-band	2.449	−0.136	0.794	0.090	0.301	0.049
$a(440)$ two-band	2.408	−0.132	0.818	0.082	0.274	0.042

[a]Computed by use of the inversion of Eq. (14) and the relationships provided in Fig. 2. Also shown are the regression results between *in situ* absorption coefficient and those predicted by use of three-band and two-band nonlinear remote-sensing reflectance models given by Lee *et al.*[26]

prediction of the absorption coefficient increases at these higher values. In fact, when considering absorption coefficients at 490 nm less than 0.15 m^{-1}, the model's ability to predict the absorption coefficient is improved (a standard error of 0.014 m^{-1}). These results emphasize that the major error in inversions to obtain the absorption coefficient is due to the assumption of the spectral dependencies of the absorption coefficient.

Linear relationships are obviously the simplest method to model the spectral dependence of the absorption coefficient. Use of more-sophisticated models that account for the individual components of the water (i.e., phytoplankton, detritus, and colored dissolved organic material) are likely to improve inversions. However, as mentioned above, our goal was not to determine the most accurate method of inverting the remotely sensed reflectance to obtain the absorption coefficient, but rather to minimize the error involved with estimating the parameters that are difficult to measure, namely, the f/Q and the b_b components.

Nevertheless it is of interest to see how this inversion algorithm compares with other algorithms based on remotely sensed reflectance ratios. Two such algorithms are provided by Lee *et al.*[26] [see their Eqs. (14) and (16)] based on empirically derived nonlinear relationships between the absorption coefficient at 440 nm and a combination of the $R_{rs}(440/555)$ and (490/555) ratios and the R_{rs} (490/555) ratio only. The *in situ* measurements of R_{rs} of the 70 profiles in this study were used as inputs to the two models given in Lee *et al.*[26] The results show that both of these nonlinear models overpredict the absorption coefficient at 443 nm to a much greater extent than the simple linear models of this paper (Table 2) and show large biases. As was found in the predicted versus measured comparisons of our inversion models, the error in the prediction of the absorption coefficient at 443 nm based on these nonlinear models was the greatest at the higher values. These results emphasize that the highest errors associated with inversion are due to the uncertainties in the spectral dependence of the absorption coefficient.

5. Discussion and Conclusions

With the development of *in situ* spectrophotometers[27,28] it is now possible to obtain absorption spectra with a high degree of accuracy (typically 0.005 m^{-1}). The accuracy of *in situ* absorption measurements and their use in radiative transfer studies and remote-sensing inversions is demonstrated in closure algorithms that compare absorption and reflectance values. We have provided a model that minimizes the dependence of the backscattering on the remote-sensing reflectance by using ratios of three wavelengths. It was shown that IOP data derived from ac-9 measurements was well correlated with the remote-sensing reflectance triple ratio from radiance and irradiance data obtained using Satlantic and Biospherical radiometers. Closure between these disparate devices has thus been demonstrated, and we have shown that radiative transfer works to within instrument accuracy.

In applications where routine instrument calibrations are limited, such as mooring deployments, this algorithm provides a method that can be used to verify or intercalibrate *in situ* IOP and AOP measurements. Remote-sensing reflectance measurements are dependent on the geometry of the incoming light field, which often makes intercomparison of AOP and IOP measurements difficult. Furthermore, the angular dependency of the backscattering coefficient is currently not well understood. The triple reflectance algorithm reduces the dependence of closure algorithms on the incoming light field and the backscattering coefficient, allowing for the intercalibration of *in situ* data that are to be used in studies of radiative transfer and remote-sensing inversions. Note that the triple reflectance algorithm is not limited to the three wavelengths used in this study. Any combination of the three wavelengths can be used provided that the spectral dependence of the backscattering coefficient of particles and the f/Q parameter is nearly linear over the wavelengths of interest. Inversion may also be possible provided that the spectral dependence of the absorption coefficient can be modeled accurately.

Nearly all semianalytical inversions of the re-

motely sensed reflectance require *a priori* knowledge of the backscattering and absorption properties of the water as well as the shape of the *in situ* light field. These models typically assume some spectral dependence of the backscattering and absorption coefficients as well as the shape of the underwater light field based on parameters such as the solar zenith angle, wind speed, and chlorophyll concentration. The focus of the current research is to minimize the number of assumptions or models needed to obtain closure between the measurements of the remotely sensed reflectance and the measured absorption coefficient. The major result of this paper is the theoretical and experimental demonstration of the equivalency of the radiometric property R_{rs3} and the IOP, the triple ratio of the absorption coefficient.

Other researchers have demonstrated the value of using reflectance ratios. Campbell and Esaias[6] showed that use of a triple ratio of reflectance removed some of the extraneous variability in the water-leaving radiance by removing most of the dependence on geometry. In fact, use of a triple ratio algorithm may also aid in removing errors associated with atmospheric correction, assuming they have nearly linear dependencies with wavelength. Our method shows utility in closure and in inversion and only assumes that the f/Q wavelength dependence is nearly linear and that the particle backscattering has a $\lambda^{-\eta}$ dependence. By one using information about the local IOP (backscattering or absorption) relationships, the inversion is possible.

Most semianalytic inversions of the remotely sensed reflectance depend on models of the spectral absorption.[3–5] These inversions usually provide models for the individual absorption components (i.e., detritus, pigment, and colored dissolved organic material). These models can be used with relation (13), and the reflectance can be inverted by minimization to obtain the absorption coefficient. Inversion to obtain the spectral absorption coefficient was demonstrated by use of simple linear relationships based on *in situ* observations. The results of the algorithm were compared with inversions of empirically derived nonlinear models based on remote-sensing reflectance ratios. Although the inversion algorithm provided in this study was shown to more accurately predict the absorption coefficient at 443 nm, it was noted that the largest error in both methods was due to the uncertainty of the spectral absorption relationships, especially in highly absorbing regimes. Improved or more-sophisticated models of the absorption coefficient are needed to obtain more-accurate inversions of the model. Use of such models should be investigated further.

Appendix A

a absorption coefficient, m^{-1};
b volume-scattering coefficient, m^{-1};
b_b backscattering coefficient, m^{-1};
$\tilde{b}_b$ probability of particle backscattering, nondimensional;

b_p scattering coefficient by particles, m^{-1};
b_{bp} backscattering coefficient of particles, m^{-1};
b_{br3} triple ratio of the backscattering coefficient at three wavelengths, nondimensional;
b_w scattering coefficient of water, m^{-1};
b_{bw} backscattering coefficient of water, m^{-1};
E_d downwelling irradiance, Wm^{-2};
E_u upwelling irradiance, Wm^{-2};
f parameter relating the reflectance to the ratio of the backscattering and absorption coefficients, nondimensional;
H_n light attenuation coefficient, nondimensional;
L_u upwelling radiance, $\mathrm{W\ m}^{-2}\ \mathrm{sr}^{-1}$;
Q the ratio of the upwelling irradiance and the nadir radiance, sr;
R irradiance reflectance, nondimensional;
R_{rs} remote-sensing reflectance: the ratio of the nadir radiance and the downwelling irradiance, sr^{-1};
R_{rs3} triple ratio of the remote-sensing reflectance at three wavelengths, nondimensional;
z depth, m;
η spectral dependence of the backscattering coefficient by particles, nondimensional; and
λ wavelength, nm.

References

1. W. S. Pegau, J. R. V. Zaneveld, and K. J. Voss, "Toward closure of the inherent optical properties of natural waters," J. Geophys. Res. **100,** 13,193–13,199 (1995).
2. W. S. Pegau, J. S. Cleveland, W. Doss, C. D. Kennedy, R. A. Maffione, J. L. Mueller, R. Stone, C. C. Trees, A. D. Weidemann, W. H. Wells, and J. R. V. Zaneveld, "A comparison of methods for the measurement of the absorption coefficient in natural waters," J. Geophys. Res. **100,** 13,201–13,220 (1995).
3. C. S. Roesler and M. J. Perry, "In situ phytoplankton absorption, fluorescence emission, and particulate backscattering spectra determined from reflectance," J. Geophys. Res. **100,** 13,279–13,294 (1995).
4. Z. P. Lee, K. L. Carder, T. G. Peacock, C. O. Davis, and J. L. Mueller, "A method to derive ocean absorption coefficients from remote-sensing reflectance," Appl. Opt. **35,** 453–462 (1996).
5. S. A. Garver and D. A. Siegel, "Inherent optical property inversion of ocean color spectra and its biogeochemical interpretation. 1. Time series from the Sargasso Sea," J. Geophys. Res. **102,** 18,607–18,625 (1997).
6. J. W. Campbell and W. E. Esaias, "Basis for spectral curvature algorithms in remote sensing of chlorophyll," Appl. Opt. **22,** 1084–1093 (1983).
7. R. W. Preisendorfer, *Hydrologic Optics* (U.S. Department of Commerce, Washington, D.C., 1976), Vol. 4.
8. H. R. Gordon, O. B. Brown, R. H. Evans, J. W. Brown, R. C. Smith, K. S. Baker, and D. K. Clark, "A semianalytic radiance model of ocean color," J. Geophys. Res. **93,** 10,909–10,924 (1988).

9. A. Morel and B. Gentili, "Diffuse reflectance of oceanic waters. II. Bidirectional aspects," Appl. Opt. **32,** 6864–6879 (1993).

10. A. Morel, K. J. Voss, and B. Gentili, "Bidirectional reflectance of oceanic waters: a comparison of modeled and measured upward radiance fields," J. Geophys. Res. **100,** 13,143–13,151 (1995).

11. A. Morel and B. Gentili, "Diffuse reflectance of oceanic waters. III. Implication of bidirectionality for the remote sensing problem," Appl. Opt. **35,** 4850–4862 (1996).

12. J. R. V. Zaneveld, "Remotely sensed reflectance and its dependence on vertical structure: a theoretical derivation," Appl. Opt. **21,** 4146–4150 (1982).

13. J. R. V. Zaneveld, "A theoretical derivation of the dependence of the remotely sensed reflectance of the ocean on the inherent optical properties," J. Geophys. Res. **100,** 13,135–13,142 (1995).

14. A. Morel, "Optical properties of pure water and pure sea water," in *Optical Aspects of Oceanography*, N. G. Jerlov and E. S. Nielsen, eds. (Academic, New York, 1974), pp. 1–24.

15. A. Morel and L. Prieur, "Analysis of variations in ocean color," Limnol. Oceanogr. **22,** 709–722 (1977).

16. R. C. Smith and K. S. Baker, "Optical properties of the clearest natural waters," Appl. Opt. **20,** 177–184 (1981).

17. A. Bricaud, A. Morel, and L. Prieur, "Optical efficiency factors of some phytoplanktors," Limnol. Oceanogr. **28,** 816–832 (1983).

18. Y. Ahn, A. Bricaud, and A. Morel, "Light backscattering efficiency and related properties of some phytoplankters," Deep-Sea Res. **39,** 1835–1855 (1992).

19. D. Stramski and D. A. Kiefer, "Light scattering by microorganisms in the open ocean," Prog. Oceanogr. **28,** 343–383 (1991).

20. R. A. Maffione and D. R. Dana, "Instruments and methods for measuring the backward-scattering coefficient of ocean waters," Appl. Opt. **36,** 6057–6067 (1997).

21. A. Morel, "Optical modeling of the upper ocean in relation to its biogenous matter content (case I waters)," J. Geophys. Res. **93,** 10,749–10,768 (1988).

22. A. H. Barnard, J. R. V. Zaneveld, and W. S. Pegau, "Global relationships of the inherent optical properties of the ocean," J. Geophys. Res. **103,** 24,955–24,968 (1998).

23. M. S. Twardowski, J. M. Sullivan, P. L. Donaghy, and J. R. V. Zaneveld, "Microscale quantification of the absorption by dissolved and particulate material in coastal waters with an ac-9," J. Atmos. Oceanic Technol. **16**(6), 691–707 (1999).

24. R. M. Pope and E. S. Fry, "Absorption spectrum (380–700 nm) of pure water. II. Integrating cavity measurements," Appl. Opt. **36,** 8710–8723 (1997).

25. J. R. V. Zaneveld and W. S. Pegau, "A model for the reflectance of thin layers, fronts, and internal waves and its inversion," Oceanography **11,** 44–47 (1998).

26. Z. P. Lee, K. L. Carder, R. G. Steward, T. G. Peacock, C. O. Davis, and J. S. Patch, "An empirical algorithm for light absorption by ocean water based on color," J. Geophys. Res. **103,** 27,967–27,978 (1998).

27. C. Moore, J. R. V. Zaneveld, and J. C. Kitchen, "Preliminary results from an in situ spectral absorption meter," in *Ocean Optics XI*, G. D. Gilbert, ed., Proc. SPIE **1750,** 330–337 (1992).

28. J. R. V. Zaneveld, J. C. Kitchen, and C. C. Moore, "Scattering error correction of reflecting tube absorption meters," in *Ocean Optics XIII*, J. S. Jaffe, ed., Proc. SPIE **2258,** 44–55 (1994).

In situ determination of the remotely sensed reflectance and the absorption coefficient: closure and inversion—errata

Andrew H. Barnard, J. Ronald V. Zaneveld, and W. Scott Pegau

In our recent paper[1] Eqs. (9) and (10) are incorrect. The correct versions of these equations are as follows:

$$b_{br3} = \frac{\left[b_{bw}(\lambda_2)\left(\frac{\lambda_1}{\lambda_2}\right)^{-4.32} + b_{bp}(\lambda_2)\left(\frac{\lambda_1}{\lambda_2}\right)^{-\eta} \right]\left[b_{bw}(\lambda_2)\left(\frac{\lambda_3}{\lambda_2}\right)^{-4.32} + b_{bp}(\lambda_2)\left(\frac{\lambda_3}{\lambda_2}\right)^{-\eta} \right]}{\left[b_{bw}(\lambda_2) + b_{bp}(\lambda_2) \right]^2}, \tag{9}$$

$$b_{br3} = \frac{\left(\frac{b_{bw}}{b_{bp}}\right)^2 \left(\frac{\lambda_1\lambda_3}{\lambda_2^{\,2}}\right)^{-4.32} + \frac{b_{bw}}{b_{bp}}\left[\left(\frac{\lambda_1}{\lambda_2}\right)^{-4.32}\left(\frac{\lambda_3}{\lambda_2}\right)^{-\eta} + \left(\frac{\lambda_1}{\lambda_2}\right)^{-\eta}\left(\frac{\lambda_3}{\lambda_2}\right)^{-4.32} \right] + \left(\frac{\lambda_1\lambda_3}{\lambda_2^{\,2}}\right)^{-\eta}}{\left(\frac{b_{bw}}{b_{bp}} + 1\right)^2}. \tag{10}$$

References

1. A. H. Barnard, J. R. V. Zaneveld, and W. S. Pegau, "*In situ* Determination of the remotely sensed reflectance and the Absorption coefficient: closure and inversion," Appl. Opt. **38,** 5108–5117 (1999).